International Journal of Solids and Structures 113–114 (2017) 180–191

Contents lists available at ScienceDirect

International Journal of Solids and Structures

journal homepage: www.elsevier.com/locate/ijsolstr

Micromechanical modelling of self-healing cementitious materials

Robert Davies*, Anthony Jefferson

Materials for Life (M4L) Research Group, School of Engineering, Cardiff University, Queen's Buildings, The Parade, Cardiff, CF24 3AA Wales, United Kingdom

ARTICLE INFO

Article history:
Received 14 December 2015
Revised 21 December 2016
Available online 17 February 2017

Keywords:
Micromechanics
Self-healing
Cementitious
Constitutive
Eshelby

ABSTRACT

A new approach is described for simulating self-healing behaviour in cementitious materials with a two phase micro-mechanical constitutive model. A Mori–Tanaka homogenisation scheme is employed for the composite along with an exterior point Eshelby solution that accounts for stress concentrations adjacent to inclusions. In addition, anisotropic micro-cracking is simulated using arrays of circular cracks. Self-healing is incorporated into the model by using a novel solidification formulation that models healing under both null and non-zero strain conditions. The focus of the present work is on the recovery of mechanical properties of the micro-cracked material. The performance of the 3D micromechanical self-healing model is illustrated using a series of stress-strain paths that involve damage and healing cycles. The implementation of the model in a layered beam model is also described, as are a series of model validations that employed data from a recent test series undertaken at Cardiff University as well as data from tests undertaken by others. The examples and validations show that the new micro-mechanical self-healing model is capable of representing the characteristic mechanical response of self-healing cementitious materials.

1. Introduction

Self-healing cementitious materials could provide a step change in the performance of concrete structures and in recent years much research has been undertaken on the subject of self-healing in cementitious materials (de Rooij et al., 2013; Van Tittelboom and De Belie, 2013).

A number of numerical models have been developed for simulating self-healing behaviour (Schlangen et al., 2006; Ye and van Breugel, 2007; Remmers and de Borst, 2008; Huang and Ye, 2012; Hilloulin et al., 2014). The majority of the mechanical healing models developed to date have been applied in finite element codes using the smeared crack concept, rather than the discrete crack approach (Perelmuter, 2013). Both macro-scale (Mergheim and Steinmann, 2013) and micro-scale (Darabi et al., 2012) models have been developed and, as with standard mechanical models, the present authors favour more mechanistic micro-mechanical models over those based on purely phenomenological relationships (Mihai and Jefferson, 2011; Davies and Jefferson, 2014).

A multiple phase self-healing model, developed by Schimmel and Remmers (2006) and Remmers and de Borst (2008), simulates three distinct stages in the healing process: fracture, transport of healing agents to the healing location and mechanical strength recovery. In this model, re-bonding of the crack surfaces was simulated by a regain of stiffness in the cohesive crack zone. A hygro-chemical transportation model was employed in their model, in which the active chemicals were assumed to be transported through the pore fluid to damage and healing sites. These transport processes can be described by advective, diffusive and dispersive fluxes (Gawin et al., 2008; Baroghel-Bouny et al., 2011). The factors governing the capillary flow of healing agents through macro-cracks in cementitious materials have been investigated by Gardner et al. (2014).

One of the first self-healing models to be based on thermodynamic principles was developed by Miao et al. (1995), who used an experimentally derived rate of healing function for crushed rock salt. Alfredsson and Stigh (2004), in their self-healing model for engineering materials, employed a damage variable based on an equivalent strain parameter that increased during continued damage but decreased when healing was simulated. In an elastoplastic-damage-healing constitutive model for fibre reinforced polymer-matrix composites, Barbero et al. (2005), used an elastic strain energy equivalence formulation to obtain a new damage-healing tensor. This concept was later extended to deal with healing in shape memory polymers (Voyiadjis et al., 2011, 2012).

A macroscopic thermodynamically consistent self-healing model for thermoset polymers was presented by Mergheim and Steinmann (2013). In their model, a healing component was added to the strain-energy density function and this was then used to

* Corresponding author.
E-mail address: daviesre11@cardiff.ac.uk (R. Davies).

http://dx.doi.org/10.1016/j.ijsolstr.2017.02.008

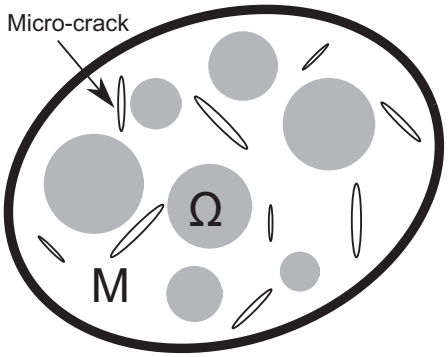

Fig. 1. Idealised components of the cementitous composite material.

develop a constitutive relationship that accounted for self-healing behaviour. These authors employed a rate equation to ensure that only the stiffness, but not the stress, increased during healing, when the strain rate was zero.

Abu Al-Rub et al. (2010) simulated healing in asphalt, subjected to fatigue loading, by applying a healing factor to the damage variable. Their micro-damage healing model combines nonlinear viscoelastic, viscoplastic and viscodamage theories and uses a phenomenological healing evolution function. The authors subsequently generalised their micro-damage healing model by formulating it within a general thermodynamic framework (Abu Al-Rub and Darabi, 2012; Darabi et al., 2013), thereby extending its range of applicability.

Many of the aforementioned constitutive models are dependent on strength properties and defined damage relationships. In cementitious materials, the development of material properties and recovery can be linked to the hydration process, particularly for early age crack healing (Schlangen et al., 2006). The chemical composition and the effect of continued hydration on self-healing processes have been investigated by Ye and van Breugel (2007) and Huang and Ye (2012) with their HYMOSTRUC3D model. This model simulates the hydration of cement particles and accounts for both water transport and ion diffusion. Although this model does consider healing, it does not simulate the associated regain of mechanical properties.

Hydration processes and damage have been considered in a coupled model developed by Granger et al. (2007b). In this work, the healing behaviour was simulated by introducing healed mechanical properties into the damaged layers of a finite beam element model. The evolution of healing was linked to both the degree of hydration and to the value of the damage parameter at time of healing. It is noted that, in this model, the evolution of damage in the newly healed material takes precedence over primary damage, which only continues in the original material when the healed material is fully damaged. This coupled model has been extended using a hygro-chemo-mechanical model for autogenous healing (Hilloulin et al., 2014).

The early stages of micro-cracking and the extent of damage in the fracture process zone around a macro-crack are difficult to capture with macro-scale models. By contrast, a micro-scale model, which considers the behaviour of the individual components of a composite, naturally captures these aspects of behaviour. Furthermore, such a model, that explicitly represents micro-cracks, provides an ideal platform from which to develop a model that includes self-healing behaviour. The authors have followed this approach and developed a new micro-mechanical model that represents self-healing behaviour. The aim of the present paper is to describe this new model, to illustrate its predictive capabilities and to provide validations based a series of experimental data.

The layout of the remainder of the paper is as follows;

- Section 2 presents the model theory.
- Section 3 describes the numerical implementation of the model.
- Section 4 presents a series of illustrative stress-strain paths that involve both damage and healing behaviour.
- Section 5 presents a series of validation examples that employ new data obtained by the authors in Cardiff University as well as data from a test series by Granger et al. (2007b).
- Section 6 gives the major conclusions from the work.

2. Micromechanical two-phase composite model with micro-crack healing

2.1. Basic constitutive model theory

A two phase composite material with inclusions (Ω) and a matrix (M) phase represent the aggregate particles and cement paste respectively in a cementitious material. The proposed model has two scales; one -the micro-scale- that relates to the maximum size of the inclusions (e.g. the size of the sand particles in mortar, or coarse aggregate particles in concrete) and the other -the macro-scale- which is the scale at which the elastic composite can reasonably considered to be homogenous. The characteristic dimension for the macro-scale is generally considered to be of the order of 5 times the maximum aggregate particle size. A more detailed description of the basic model and further discussion of these scales may be found in Mihai and Jefferson (2011), 2013) and Davies and Jefferson (2014). The components of the composite, including micro-cracks, are shown in Fig. 1.

The average stress and strain tensors are given by $\bar{\boldsymbol{\sigma}}$ and $\bar{\boldsymbol{\varepsilon}}$ respectively, and the sum of the volume fractions (f_Ω and f_M) is unity. The elastic properties of the two-phase composite are computed using the classical Eshelby (1957) solution and the Mori–Tanaka homogenisation scheme for non-dilute inclusions (Mori and Tanaka, 1973; Benveniste, 1987). The additional strain resulting from anisotropic micro-cracking is taken into account using the approach of Budiansky and O'Connell (1976). Combining these model components gives the following constitutive equation;

$$\bar{\boldsymbol{\sigma}} = \mathbf{D}_{\mathrm{M}\Omega} : (\bar{\boldsymbol{\varepsilon}} - \boldsymbol{\varepsilon}_{\mathrm{a}}) \tag{1}$$

where $\mathbf{D}_{\mathrm{M}\Omega} = (f_\Omega \mathbf{D}_\Omega \cdot \mathbf{T}_\Omega + f_M \mathbf{D}_{\mathrm{M}}) \cdot \left(f_\Omega \mathbf{T}_\Omega + \mathbf{I}^{4s} f_M\right)^{-1}$ is the composite elasticity tensor, $\mathbf{T}_\Omega = \mathbf{I}^{4s} + \mathbf{S} \cdot \mathbf{A}_\Omega$ and $\mathbf{A}_\Omega = [(\mathbf{D}_\Omega - \mathbf{D}_{\mathrm{M}}) \cdot \mathbf{S} + \mathbf{D}_{\mathrm{M}}]^{-1} \cdot (\mathbf{D}_{\mathrm{M}} - \mathbf{D}_\Omega)$. $\mathbf{D}_\Omega$ and $\mathbf{D}_{\mathrm{M}}$ are the elastic tensors for the inclusion and matrix phases respectively. $\mathbf{S}$ is the interior point fourth order Eshelby tensor (Nemat-Nasser and Hori, 1999), $\mathbf{I}^{4s}$ is the fourth order identity tensor and $\boldsymbol{\varepsilon}_{\mathrm{a}}$ is the total added strain.

The added strains in Eq. (1) are the sum (integral) of the added strains on sets of micro-cracks with common directions, as explained below. The formation of these micro-cracks depends initially upon the maximum stress computed at the matrix-inclusion boundary and these micro-cracks subsequently evolve according to an effective local strain parameter (See Section 2.6 and Mihai and Jefferson (2011)). This approach differs somewhat from methods in which micro-cracks are represented as empty shallow ellipsoid inclusions incorporated into the idealised composite via a homogenisation scheme (e.g. Mori–Tanaka) (Pichler et al., 2007). In the present approach, Mori–Tanaka homogenisation is only used to compute the elastic properties of the two-phase composite. The advantage of the approach adopted here is that the formulation simulates the evolution of the micro-cracked composite as a generally anisotropic material, and places no restrictions on the degree or type of anisotropy.

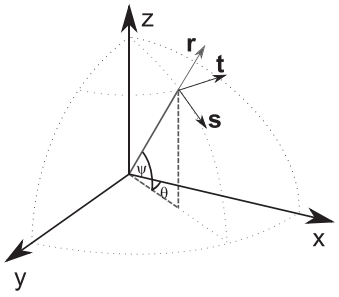

Fig. 2. Reference system for crack planes.

In a single direction, the additional strain from circular micro-cracks (Budiansky and O'Connell, 1976), is shown in Eq. (2);

$$\boldsymbol{\varepsilon}_\alpha = f\frac{16\left(1-\nu_M{}^2\right)}{3E_M}\begin{bmatrix} \sigma_{rr} \\ \frac{4}{2-\nu_M}\sigma_{rs} \\ \frac{4}{2-\nu_M}\sigma_{rt} \end{bmatrix} \tag{2}$$

where f is the crack density parameter. ν_M and E_M are Poisson's ratio and Young's modulus of the matrix material respectively. $\mathbf{r}$, $\mathbf{s}$ and $\mathbf{t}$ define the unit local coordinate vectors, with $\mathbf{r}$ being the vector normal to the micro-crack surface, and $\mathbf{s}$ & $\mathbf{t}$ being orthogonal vectors in the plane of the surface, as shown in Fig. 2 for a single direction.

Jefferson and Bennett (2007) showed that there was a direct equivalence between Budiansky and O'Connell's crack density parameter (f) and a directional micro-cracking $\omega \in [0, 1]$, as given in Eq. (3);

$$f = \frac{3}{16\left(1-\nu_M{}^2\right)}\left(\frac{\omega}{1-\omega}\right) \tag{3}$$

A local stress-strain relationship for the micromechanical model is defined in Eq. (4), in which the added strain is taken to be the equivalent of a micro-cracked band in the material. $\mathbf{s}_\mathrm{L}$ is the equivalent local stress tensor and $\boldsymbol{\varepsilon}_\mathrm{L}$ is the equivalent local strain tensor, both of which are expressed in a reduced vector form that considers only those components that can be non-zero. $\mathbf{s}_\mathrm{L}$ is related to $\bar{\boldsymbol{\sigma}}$ using the stress transformation tensor ($\mathbf{N}$) given in Eq. (5). Similarly, the strain transformation tensor ($\mathbf{N}_\varepsilon$) relates the local strain to the composite average strain ($\bar{\boldsymbol{\varepsilon}}$). $\mathbf{N}$ and $\mathbf{N}_\varepsilon$ are the transformation tensors given by Jefferson (2003). $\mathbf{D}_\mathrm{L}$ is expressed as a 3x3 matrix that contains the non-zero components of the local stiffness tensor and $\mathbf{C}_\mathrm{L}$ is the associated local elastic compliance tensor, as shown in Eq. (6).

$$\mathbf{s}_\mathrm{L} = (1-\omega)\mathbf{D}_\mathrm{L} : \boldsymbol{\varepsilon}_\mathrm{L} \tag{4}$$

$$\mathbf{s}_\mathrm{L} = \begin{bmatrix} \sigma_{rr} & \sigma_{rs} & \sigma_{rt} \end{bmatrix}^T = \mathbf{N}\cdot\bar{\boldsymbol{\sigma}} \tag{5}$$

$$\mathbf{D}_\mathrm{L} = \mathbf{C}_\mathrm{L}{}^{-1} = E_M\begin{bmatrix} 1 & 0 & 0 \\ 0 & \frac{2-\nu_M}{4} & 0 \\ 0 & 0 & \frac{2-\nu_M}{4} \end{bmatrix} \tag{6}$$

Using the above definitions, $\boldsymbol{\varepsilon}_\alpha$ in Eq. (2), can be expressed in terms of the local strain within the micro-crack band ($\boldsymbol{\varepsilon}_\mathrm{L}$) and elastic local strain ($\boldsymbol{\varepsilon}_\mathrm{Le}$) as follows;

$$\boldsymbol{\varepsilon}_\alpha = \boldsymbol{\varepsilon}_\mathrm{L} - \boldsymbol{\varepsilon}_\mathrm{Le} = \left(\frac{1}{1-\omega}-1\right)\mathbf{C}_\mathrm{L} : \mathbf{s}_\mathrm{L} = \left(\frac{\omega}{1-\omega}\right)\mathbf{C}_\mathrm{L} : \mathbf{s}_\mathrm{L} \tag{7}$$

The total added strain ($\boldsymbol{\varepsilon}_\mathrm{a}$) in Eq. (8) is obtained by integrating the added strain contributions from all directions around a hemisphere (Nemat-Nasser and Hori, 1999). McLaren's integration rule with 29 sample directions is used to evaluate this integration numerically (Stroud, 1972). Noting that $\mathbf{N}$, $\mathbf{N}_\varepsilon$ and ω are functions of the spherical coordinate angles (θ, ψ).

$$\boldsymbol{\varepsilon}_\mathrm{a} = \left(\frac{1}{2\pi}\int_{2\pi}\int_{\frac{\pi}{2}} \mathbf{N}_\varepsilon\cdot\mathbf{C}_\mathrm{L}\cdot\mathbf{N}\cdot\frac{\omega(\theta,\psi)}{1-\omega(\theta,\psi)}sin(\psi)\mathrm{d}\psi\mathrm{d}\theta\right) : \bar{\boldsymbol{\sigma}} \tag{8}$$

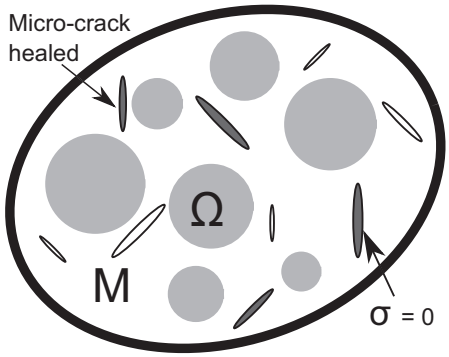

Fig. 3. Micro-crack healing.

2.2. Addition of healing into the local constitutive model

Healing is incorporated into the local constitutive relationship (i.e. for a particular direction) by restoring the stiffness of a proportion of the damaged component of material and including an offset or 'solidification' strain. The healing proportion is defined by the parameter $h \in [0, 1]$ and the 'solidification strain' ($\boldsymbol{\varepsilon}_\mathrm{s}$) is included to ensure that the healing material solidifies in a stress free state. This is illustrated in Fig. 3. The local stress is now given by;

$$\mathbf{s}_\mathrm{Lh} = (1-\omega)\mathbf{D}_\mathrm{L} : \boldsymbol{\varepsilon}_\mathrm{Lh} + h\omega_{th}\mathbf{D}_\mathrm{Lh} : (\boldsymbol{\varepsilon}_\mathrm{Lh} - \boldsymbol{\varepsilon}_\mathrm{s}) \tag{9}$$

in which $\mathbf{s}_\mathrm{Lh}$ is the equivalent local stress tensor after healing, $\boldsymbol{\varepsilon}_\mathrm{Lh}$ is the equivalent local strain tensor after healing, $\mathbf{D}_\mathrm{Lh}$ is the local stiffness of the healed material and ω_{th} is the micro-cracking parameter at the time of healing.

2.3. Additional strain due to microcracks and healing

An expression for the local equivalent strain may be obtained by rearranging Eq. (9) as follows;

$$\boldsymbol{\varepsilon}_\mathrm{Lh} = \left[(1-\omega) + h\omega_{th}B\right]^{-1}\mathbf{C}_\mathrm{L} : (\mathbf{s}_\mathrm{Lh} + h\omega_{th}B\mathbf{D}_\mathrm{L} : \boldsymbol{\varepsilon}_\mathrm{s}) \tag{10}$$

where $\mathbf{D}_\mathrm{Lh} = B\cdot\mathbf{D}_\mathrm{L}$ and B (a material parameter) is the ratio between the stiffness of the healed and original material.

The added inelastic strain for the healed band of material in each direction is obtained by subtracting the elastic component of strain from $\boldsymbol{\varepsilon}_\mathrm{Lh}$, as follows;

$$\boldsymbol{\varepsilon}_{\alpha\mathrm{h}} = \boldsymbol{\varepsilon}_\mathrm{Lh} - \boldsymbol{\varepsilon}_\mathrm{Le} \tag{11}$$

Substituting for $\boldsymbol{\varepsilon}_\mathrm{Lh}$ from Eq. (10) and $\boldsymbol{\varepsilon}_\mathrm{Le}$ from $\boldsymbol{\varepsilon}_\mathrm{Le} = \mathbf{C}_\mathrm{L} : \mathbf{s}_\mathrm{L}$ in (11) and rearranging results in Eq. (12) for the added local stain with healing, noting that this is the healing equivalent of Eq. (7).

$$\boldsymbol{\varepsilon}_{\alpha\mathrm{h}} = \left(\frac{\omega - h\omega_{th}B}{1-\omega+h\omega_{th}B}\right)\mathbf{C}_\mathrm{L} : \mathbf{s}_\mathrm{Lh} + \left(\frac{h\omega_{th}B}{1-\omega+h\omega_{th}B}\right)\boldsymbol{\varepsilon}_\mathrm{s} \tag{12}$$

The total added strain is, as in Eq. (8), obtained by integrating the contributions from the two components of $\boldsymbol{\varepsilon}_{\alpha\mathrm{h}}$ as follows;

$$\boldsymbol{\varepsilon}_{\mathrm{ah}} = \boldsymbol{\varepsilon}_{\mathrm{ac}} + \boldsymbol{\varepsilon}_{\mathrm{as}} \tag{13}$$

where

$$\boldsymbol{\varepsilon}_{\mathrm{ac}} = \left[\frac{1}{2\pi}\int_{2\pi}\int_{\frac{\pi}{2}} \mathbf{N}_\varepsilon\cdot\mathbf{C}_\mathrm{L}\cdot\mathbf{N}\left(\frac{\omega - h\omega_{th}B}{1-\omega+h\omega_{th}B}\right)\sin(\psi)\mathrm{d}\psi\mathrm{d}\theta\right] : \bar{\boldsymbol{\sigma}} \tag{14}$$

and

$$\boldsymbol{\varepsilon}_{as} = \left[\frac{1}{2\pi}\int_{2\pi}\int_{\frac{\pi}{2}} \mathbf{N}_{\varepsilon}\cdot\left(\frac{h\omega_{th}B}{1-\omega+h\omega_{th}B}\right)\sin(\psi)\mathrm{d}\psi\mathrm{d}\theta\right]\boldsymbol{\varepsilon}_{s} \tag{15}$$

Substituting the total added strain component contributions from Eq. (14) and (15) into Eq. (1) leads to the following overall constitutive relationship;

$$\bar{\boldsymbol{\sigma}} = \left(\mathbf{I}^{4s} + \mathbf{D}_{M\Omega}\cdot\mathbf{C}_{addh}\right)^{-1}\cdot\mathbf{D}_{M\Omega} : (\bar{\boldsymbol{\varepsilon}} - \boldsymbol{\varepsilon}_{as}) \tag{16}$$

where

$$\mathbf{C}_{addh} = \frac{1}{2\pi}\int_{2\pi}\int_{\frac{\pi}{2}} \mathbf{N}_{\varepsilon}\cdot\mathbf{C}_{L}\cdot\mathbf{N}\left(\frac{\omega-h\omega_{th}B}{1-\omega+h\omega_{th}B}\right)\sin(\psi)\mathrm{d}\psi\mathrm{d}\theta \tag{17}$$

2.4. Determining the solidification strain

The deposition of healed material is assumed to take place in a stress free state, and therefore the overall stress in the composite is assumed not to change at the moment of healing. The same assumptions were used by Bažant and Prasannan (1989) in their solidification creep model when considering the stress in newly formed material during early age hydration. In order to satisfy these assumptions in the present model, the local solidification strain is made equal to the local strain at the time of healing, i.e. $\boldsymbol{\varepsilon}_s = \boldsymbol{\varepsilon}_{Lth}$. Using this assumption in Eq. (9) results in the following expression;

$$\begin{aligned}\mathbf{s}_{Lth} &= (1-\omega_{th})\mathbf{D}_{L} : \boldsymbol{\varepsilon}_{Lth} + h\omega_{th}\mathbf{D}_{Lh} : (\boldsymbol{\varepsilon}_{Lth} - \boldsymbol{\varepsilon}_{s}) \\ &= (1-\omega_{th})\mathbf{D}_{L} : \boldsymbol{\varepsilon}_{Lth} + 0\end{aligned} \tag{18}$$

in which ω_{th} is the micro-cracking damage parameter at the time of healing and $\mathbf{s}_{Lth}$ is the local stress at the time of healing. Eq. (18) is now rearranged to give the solidification strain, as follows;

$$\boldsymbol{\varepsilon}_{s} = \left(\frac{1}{1-\omega_{th}}\right)\mathbf{C}_{L} : \mathbf{s}_{Lth} \tag{19}$$

with $\mathbf{s}_{Lth}$ being obtained from the transformed macro-scopic stress at the time of healing i.e. $\mathbf{s}_{Lth} = \mathbf{N}\bar{\boldsymbol{\sigma}}$.

2.5. Continuing damage of healed material

This newly healed composite material may itself undergo micro-cracking. This is simulated by the introduction of the healed-material micro-cracking parameter (ω_h) into the local stress equation as follows;

$$\mathbf{s}_{Lh} = (1-\omega)\mathbf{D}_{L} : \boldsymbol{\varepsilon}_{Lh} + (1-\omega_h)h\omega_{th}B\mathbf{D}_{L} : (\boldsymbol{\varepsilon}_{Lh} - \boldsymbol{\varepsilon}_{s}) \tag{20}$$

It is noted that this formulation allows different material parameters to be used in the micro-crack initiation and evolution criteria for the original and healed material. Fig. 4 shows the considered microstructure with continuing micro-cracking.

Applying the same steps followed in Section 2.3, but now allowing for micro-cracking in the healed material, leads to Eq. (21) for the added local strain.

$$\boldsymbol{\varepsilon}_{\alpha h\omega} = \left(\frac{\omega-(1-\omega_h)h\omega_{th}B}{1-\omega+(1-\omega_h)h\omega_{th}B}\right)\mathbf{C}_{L} : \mathbf{s}_{Lh} + \left(\frac{(1-\omega_h)h\omega_{th}B}{1-\omega+(1-\omega_h)h\omega_{th}B}\right)\boldsymbol{\varepsilon}_{s} \tag{21}$$

The resulting two components of the total added strain (see Eq. (13)) are now given by;

$$\boldsymbol{\varepsilon}_{ac\omega} = \left[\frac{1}{2\pi}\int_{2\pi}\int_{\frac{\pi}{2}} \mathbf{N}_{\varepsilon}\cdot\mathbf{C}_{L}\cdot\mathbf{N}\left(\frac{\omega-(1-\omega_h)h\omega_{th}B}{1-\omega+(1-\omega_h)h\omega_{th}B}\right)\sin(\psi)\mathrm{d}\psi\mathrm{d}\theta\right] : \bar{\boldsymbol{\sigma}} \tag{22}$$

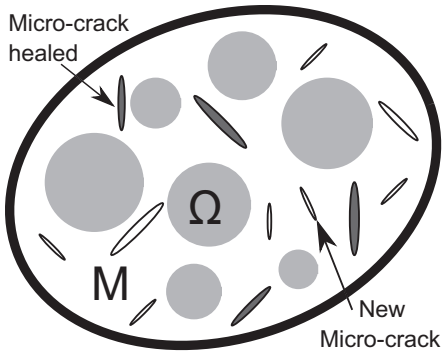

Fig. 4. Post-healing showing new micro-cracks and cracking of healed material.

and

$$\boldsymbol{\varepsilon}_{as\omega} = \left[\frac{1}{2\pi}\int_{2\pi}\int_{\frac{\pi}{2}} \mathbf{N}_{\varepsilon}\left(\frac{(1-\omega_h)h\omega_{th}B}{1-\omega+(1-\omega_h)h\omega_{th}B}\right)\sin(\psi)\mathrm{d}\psi\mathrm{d}\theta\right]\boldsymbol{\varepsilon}_{s} \tag{23}$$

Using Eqs. (22) and (23) in the overall constitutive relationship, in place of Eqs. (14) and (15), leads to the following constitutive equations, which are the counterparts to Eqs. (16) and (17).

$$\bar{\boldsymbol{\sigma}} = \left(\mathbf{I}^{4s} + \mathbf{D}_{M\Omega}\cdot\mathbf{C}_{addh\omega}\right)^{-1}\cdot\mathbf{D}_{M\Omega} : (\bar{\boldsymbol{\varepsilon}} - \boldsymbol{\varepsilon}_{as\omega}) \tag{24}$$

in which

$$\mathbf{C}_{addh\omega} = \frac{1}{2\pi}\int_{2\pi}\int_{\frac{\pi}{2}} \mathbf{N}_{\varepsilon}\cdot\mathbf{C}_{L}\cdot\mathbf{N}\left(\frac{\omega-(1-\omega_h)h\omega_{th}B}{1-\omega+(1-\omega_h)h\omega_{th}B}\right)\sin(\psi)\mathrm{d}\psi\mathrm{d}\theta \tag{25}$$

2.6. Micro-crack criterion and evolution

The original and healed micro-cracking initiation and evolution criteria are based on the following form adopted by Mihai and Jefferson (2011);

$$\sigma_{\beta} = f_{t\beta}e^{-c_{\beta}\frac{\zeta_{\beta}-\varepsilon_{t\beta}}{\varepsilon_{0\beta}-\varepsilon_{t\beta}}} \tag{26}$$

in which subscript β denotes the material undergoing micro-cracking, i.e. the original matrix material (d) or healing material (dh), c_{β} is a constant taken to be 5 and $f_{t\beta}$ is a local tensile strength. ζ_{β} is an effective local strain parameter, which is initialised to $\varepsilon_{t\beta}$ and is updated whenever the previous maximum value is exceeded. $\varepsilon_{t\beta}$ is the strain at first uniaxial micro-cracking and is taken as;

$$\varepsilon_{t\beta} = \frac{f_{t\beta}}{E_{\beta}} \tag{27}$$

in which E_d is Young's modulus of the matrix and E_{dh} is Young's modulus of the healed material. $\varepsilon_{0\beta}$ is an uniaxial local strain in the effectively fully micro-cracked state and is assumed to be related to the associated relative-displacements by the following relationship;

$$\varepsilon_{0\beta} = \frac{u_{0\beta}}{h_{\beta}} \tag{28}$$

in which h_{β} is assumed to be 3 times the size of the coarse aggregate particles. These are typically 10 mm in diameter for laboratory concrete and 20 mm for structural concrete. The relative displacement at the fully micro-cracked state for $u_{0\beta}$ is taken as 0.2 mm (Reinhardt, 1984).

The onset of micro-cracking is controlled by the elastic stress field in a narrow band of material adjacent to a coarse aggregate particle (Mihai and Jefferson, 2011). The micro-cracking initiation criterion for the directional component is reached when the local

Table 1
Computational algorithm for iterative local micro-cracking to update stress after healing.

Enter with $\bar{\boldsymbol{\varepsilon}}$, $\bar{\boldsymbol{\varepsilon}}_{\text{prv}}$, $\zeta_{\beta_{prv}}$, $\Delta\boldsymbol{\sigma}$, $\Delta\boldsymbol{\varepsilon}$ For $t = t_{heal}$ to t_{ns}	Enter with stress/strains increments and previous equivalent strain parameters
If *Healed* = *false*	Time of healing
For $i = 1$ to n_i	Loop over integration directions
$\boldsymbol{\varepsilon}_{\text{s}_i} = (1-\omega_{th_i})^{-1}\mathbf{C}_{\text{LM}\Omega} : \mathbf{N}_i \cdot \bar{\boldsymbol{\sigma}}$	Evaluate local solidification strain vector
Healed = *true*	
End if	
If *Healed* = *true*	Post-healing
For $i = 1$ to n_i	Loop over integration directions
$\boldsymbol{\varepsilon}_{\text{M}\Omega}(\mathbf{x}) = \mathbf{T}^E(\mathbf{x}) : \boldsymbol{\varepsilon}_{\text{M}}$	Compute matrix strain (EPE)
$\mathbf{s}_{\text{M}\Omega\text{d}}(\mathbf{x}) = \mathbf{N}_i \cdot \mathbf{D}_{\text{M}} : \boldsymbol{\varepsilon}_{\text{M}\Omega}(\mathbf{x})$	Compute local cracking stress in the original material
If $s_{Id}(\mathbf{s}_{\text{M}\Omega\text{d}}(\mathbf{x}))_{\max} \le f_{td}$ then $\omega_i = 0$	Micro-crack initiation criterion
Else	Micro-crack evolution
$\boldsymbol{\varepsilon}_{\text{L}_i} = (1-\omega_i)\mathbf{C}_{\text{LM}} : \mathbf{s}_{\text{M}\Omega\text{d}}(\mathbf{x}) + \omega_i \mathbf{N}_{\varepsilon_i} \cdot \bar{\boldsymbol{\varepsilon}}$	Evaluate local strain vector
$\zeta_{d_i} = F_{\zeta_d}(\boldsymbol{\varepsilon}_{\text{L}_i})$ if $\zeta_{d_i} > \zeta_{dprv_i}$	Update effective local strain parameter, if required
Update ω_i	Update damage parameter
End if	
$\mathbf{s}_{\text{M}\Omega dh}(\mathbf{x}) = \mathbf{N}_i \cdot B \cdot \mathbf{D}_{\text{M}} : \boldsymbol{\varepsilon}_{\text{M}\Omega}(\mathbf{x})$	Compute local cracking stress in healed material
If $s_{Idh}(\mathbf{s}_{\text{M}\Omega dh}(\mathbf{x}))_{\max} \le f_{tdh}$ then $\omega_{h_i} = 0$	Micro-crack initiation criterion
Else	Micro-crack evolution
$\boldsymbol{\varepsilon}_{\text{Lh}_i} = (1-\omega_{h_i})B^{-1}\mathbf{C}_{\text{LM}} : \mathbf{s}_{\text{M}\Omega dh}(\mathbf{x}) + \omega_{h_i}\mathbf{N}_{\varepsilon_i} \cdot \bar{\boldsymbol{\varepsilon}}$	Evaluate local strain vector
$\zeta_{dh_i} = F_{\zeta_{dh}}(\boldsymbol{\varepsilon}_{\text{Lh}_i} - \boldsymbol{\varepsilon}_{\text{s}_i})$ if $\zeta_{dh_i} > \zeta_{dhprv_i}$	Update strain parameter in healed material, if required
Update ω_{h_i}	Update damage parameter
End if	
End if	
$\mathbf{C}_{\text{addh}\omega} = \sum_{i=1}^{n_i} \mathbf{N}_{\varepsilon_i} \cdot \mathbf{C}_{\text{LM}\Omega} \cdot \mathbf{N}_i \frac{\omega_i - (1-\omega_{h_i})h\omega_{ht_i}B}{1-\omega_i+(1-\omega_{h_i})h\omega_{ht_i}B} \text{w}_i$	Evaluate total added compliance
$\boldsymbol{\varepsilon}_{\text{as}\omega} = \sum_{i=1}^{n_i} \mathbf{C}_{\text{LM}\Omega} \cdot \mathbf{N}_i \frac{(1-\omega_{h_i})h\omega_{ht_i}B}{1-\omega_i+(1-\omega_{h_i})h\omega_{ht_i}B} \text{w}_i \boldsymbol{\varepsilon}_{\text{Lh}_i}$	Evaluate total solidification strain contribution
$\mathbf{D}_{\text{Sech}\omega} = \left(\mathbf{I}^{4s} + \mathbf{D}_{\text{M}\Omega} \cdot \mathbf{C}_{\text{addh}\omega}\right)^{-1} \cdot \mathbf{D}_{\text{M}\Omega}$	Form secant constitutive matrix
$\bar{\boldsymbol{\sigma}} = \mathbf{D}_{\text{Sech}\omega} : (\bar{\boldsymbol{\varepsilon}} - \boldsymbol{\varepsilon}_{\text{as}\omega})$	Compute stresses

principal stress ($s_{I\beta}$), given by Eq. (29), exceeds the initial interface tensile strength ($f_{t\beta}$).

$$s_{I\beta} = s_{rr}\left(\frac{1+\alpha_L}{2}\right) + \sqrt{{s_{rr}}^2\left(\frac{1-\alpha_L}{2}\right)^2 + {\tau_L}^2} \tag{29}$$

where $\alpha_L = \left(\frac{\nu_M}{1-\nu_M}\right)$ and $\tau_L = \sqrt{{s_{rs}}^2 + {s_{rt}}^2}$, in which $\mathbf{s} = \mathbf{s}_{\text{M}\Omega\beta}$ is the transformed amplified stress adjacent to an inclusion (Mihai and Jefferson, 2011), as defined in Eq. (37). Once formed, the extent of micro-cracking is expressed in terms of the damage parameter (ω_β), which is given by;

$$\omega_\beta = 1 - \frac{\varepsilon_{t\beta}}{\zeta_\beta} e^{-c_\beta\left(\frac{\zeta_\beta - \varepsilon_{t\beta}}{\varepsilon_{0\beta} - \varepsilon_{t\beta}}\right)} \tag{30}$$

This relationship depends on the effective local strain parameter (ζ_β), which is governed by the directional micro-cracking function (31).

$$F_{\zeta_\beta}(\boldsymbol{\varepsilon}_{L\beta}, \zeta_\beta) = \boldsymbol{\varepsilon}_{L_{rr}}\left(\frac{1+\alpha_L}{2}\right) + \sqrt{{\boldsymbol{\varepsilon}_{L_{rr}}}^2\left(\frac{1-\alpha_L}{2}\right)^2 + {r_\zeta}^2\gamma^2} - \zeta_\beta \tag{31}$$

where $\gamma = \sqrt{{\boldsymbol{\varepsilon}_{L_{rs}}}^2 + {\boldsymbol{\varepsilon}_{L_{rt}}}^2}$ and $r_\zeta = \left(\frac{\nu_M - 1/2}{\nu_M - 1}\right)$. These functions are subject to the standard loading/ unloading conditions as follows;

$$F_{\zeta_\beta} \le 0; \qquad \dot{\zeta_\beta} \ge 0; \qquad F_{\zeta_\beta}\dot{\zeta_\beta} = 0 \tag{32}$$

The directional local strain ($\boldsymbol{\varepsilon}_{\text{L}}$) is assumed equal to the sum of the peak elastic strain in the matrix phase ($\boldsymbol{\varepsilon}_{\text{LMe}}$), based on $\mathbf{s}_{\text{M}\Omega\beta}$, and the local micro-cracking strain ($\boldsymbol{\varepsilon}_\alpha$), as shown in (33) (Mihai and Jefferson, 2011).

$$\boldsymbol{\varepsilon}_{\text{L}} = \boldsymbol{\varepsilon}_{\text{LMe}} + \boldsymbol{\varepsilon}_\alpha \tag{33}$$

where

$$\boldsymbol{\varepsilon}_{\text{LMe}} = (1-\omega_\beta)\mathbf{C}_{\text{L}} : \mathbf{s}_{\text{M}\Omega\beta} \tag{34}$$

and

$$\boldsymbol{\varepsilon}_\alpha = \omega_\beta \mathbf{N}_\varepsilon \cdot \bar{\boldsymbol{\varepsilon}}_e = \omega_\beta \mathbf{N}_\varepsilon \cdot \bar{\boldsymbol{\varepsilon}} \tag{35}$$

The micro-cracking function in the matrix is based on $\boldsymbol{\varepsilon}_{\text{L}}$ whereas that for the healed material depends upon $\boldsymbol{\varepsilon}_{\text{L}} - \boldsymbol{\varepsilon}_{\text{s}}$, which takes account of the solidification strain.

The exterior point Eshelby solution (Ju and Sun, 1999) is used to give the stress and strain amplification at any point in the matrix. The stress tensor in the matrix on each local plane for the original material before healing is given by Eq. (37) and for the healed material is given by Eq. (38). The stress in the healed material is directly related to the ratio B.

$$\boldsymbol{\varepsilon}_{\text{M}\Omega}(\mathbf{x}) = \left(\mathbf{I}^{4s} + \mathbf{S}^E(\mathbf{x}) \cdot \mathbf{A}_\Omega\right) : \boldsymbol{\varepsilon}_{\text{M}} \tag{36}$$

$$\boldsymbol{s}_{\text{M}\Omega\text{d}}(\mathbf{x}) = \mathbf{N} \cdot \mathbf{D}_{\text{M}} : \boldsymbol{\varepsilon}_{\text{M}\Omega}(\mathbf{x}) \tag{37}$$

$$\boldsymbol{s}_{\text{M}\Omega\text{dh}}(\mathbf{x}) = \mathbf{N} \cdot B \cdot \mathbf{D}_{\text{M}} : \boldsymbol{\varepsilon}_{\text{M}\Omega}(\mathbf{x}) \tag{38}$$

where $\mathbf{S}^E(\mathbf{x})$ is the exterior point Eshelby tensor (Ju and Sun, 1999; Mihai and Jefferson, 2011). $\mathbf{x}$ is the position vector from the centre of a spherical aggregate particle, $\rho = a/|\mathbf{x}|$ is the relative distance taken as 0.999, $|\mathbf{x}| = \sqrt{x_i x_i}$ is the position vector and a is the radius of the spherical inclusion.

For the autogenous healing case in concrete, the healed material is likely to be weaker than the original material (Granger et al., 2005). The introduction of this weaker material into the micro-cracks will have little effect on the original material stiffness because the volume of the healed material is very small in comparison with the total material volume. The effects of micro-crack healing are explored using illustrative examples in Section 4.

Table 2
Material properties for characteristic model.

f_M	E_M (N/mm^2)	ν_M	f_Ω	E_Ω (N/mm^2)	ν_Ω	f_t (N/mm^2)
0.3	20,000	0.15	0.7	55,000	0.25	1
ε_t	ε_0	f_{th} (N/mm^2)	ε_{th}	ε_{0h}	h	B
$5\ x10^{-5}$	0.067	$p \cdot f_t$	$f_{th}/B \cdot E_M$	$p \cdot \varepsilon_0$	$p \cdot 0.5$	$p \cdot 0.5$

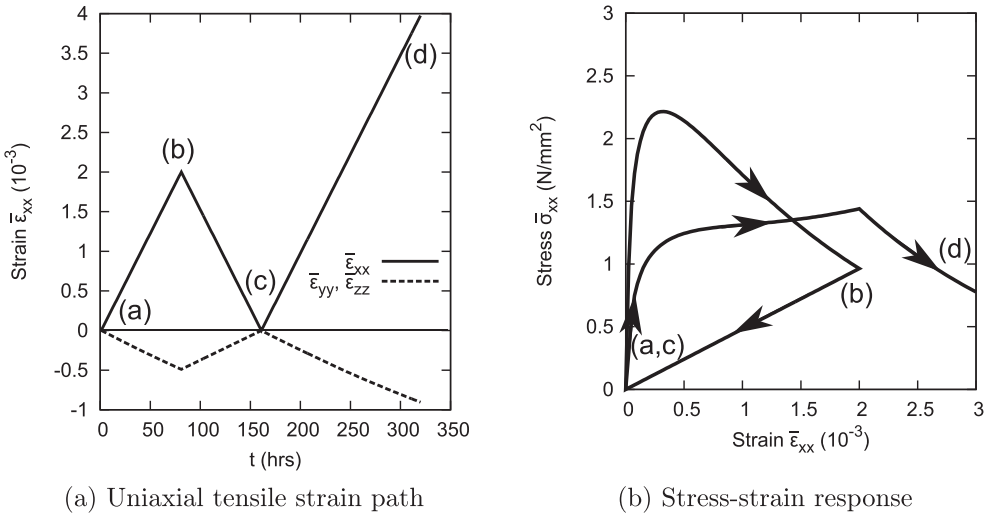

(a) Uniaxial tensile strain path (b) Stress-strain response

Fig. 5. Model response with standard material properties.

3. Numerical implementation

The self-healing micromechanical model, presented in the previous section, has been implemented in a Mathcad (2010) sheet using a constitutive driver algorithm. The model follows a specified path, which is defined by stress and/or strain increments (i.e. $\Delta\boldsymbol{\sigma}$, $\Delta\boldsymbol{\varepsilon}$ respectively) (Davies, 2014). The simulation considers the period of time before healing occurs (t_0 to t_{heal}), the moment of healing (t_{heal}) as well as the post-healing phase (t_{heal} to t_{ns}). The computational algorithm for the post-healed stress update is shown in Table 1.

4. Characteristic model predictions

The characteristic performance of the model is illustrated for a series of stress-strain paths that involve both micro-cracking and healing. This analysis series includes a parametric study that explores the effects of varying key parameters on the response computed by the model. This is followed by a 3D example in which the material is strained uniaxially whilst being constrained in the other directions. The material properties used in these illustrations are given in Table 2. In the parametric study, the healed local tensile strength (f_{th}) at the aggregate/cement paste interface, the effective uniaxial strain (ε_{0h}) at the end of the characteristic softening curve, the healing efficiency (h) and the healing strength ratio (B) are varied one at time using ratio p (which takes the values 0.25, 0.5, 1 and 2). The same micro-cracking function is used for both original and healed materials. The full 3D model, with 29 sample directions for the spherical integrals (Eqs. (24) and (25)), is used for all simulations. The unit direction vectors and weightings for these sampling directions are given in Appendix A.

The results from an analysis for a cyclic uniaxial tensile strain path, using the reference material parameters, are shown in Fig. 5. In this example, healing is assumed to take place at a time of 160 hours (i.e. at point c on the graphs in Figs. 5a and b, when the x-x strain component ($\bar{\varepsilon}_{xx}$) is zero. $\bar{\varepsilon}_{xx}$ is increased linearly (with respect to time) during the reloading phase, shown in Fig. 5a, during which the stress response is shown to have two distinct gradients up to the post-healed peak stress, as may be seen in Fig. 5b. The steep gradient, at the start of this reloading (i.e. loading after healing) phase, reflects the stiffness of the healed material, whilst the flatter gradient of the following section results from a combination of micro-cracking in the newly healed material and the original material taking stress without further micro-cracking. In the final section (with a negative gradient i.e. from point d) the level of micro-cracking is increasing in both the newly healed and original material. The associated micro-cracking parameter response is given in Fig. 6 for two selected directions (i.e. ω_1 and ω_{17} which have the unit vectors r_1 and r_{17}).

The results of the parametric study are shown in Fig. 7. Fig. 7a shows the influence of changing the ratio between f_t and f_{th} (i.e. $f_{th} = p \cdot f_t$) on the stress-strain response. It is noted that since f_t remains constant for all analysis, the pre-healing response (i.e. a to b) is the same for all cases. The first observation from the parametric study is that, as expected, the post-healing response transitions from the no healing case, shown as p=0 in Fig. 7a, to the maximum healing responses (given by p=2 in Fig. 7a and Fig. 7c) as the strength (Fig. 7a) and efficiency (Fig. 7c) of the healed zone is increased, i.e. as p increases from 0 to 2. It may be seen that even when the healing material has a strength $^1/_4$ that of the parent material (p=0.25 in Fig. 7a), there is still significant healing, indicated by a greater initial slope than the p=0 case. Even for these p=0.25 cases (Fig. 7a and 7 c), the effects of the gradual micro-cracking of the healed material is still evident in the reloading responses, which show significant nonlinearity up to the reloading peak. The effect of varying the limiting strain (ε_{0h}) on the response is also very significant and it may be seen from Fig. 7b that for a small ε_{0h} (when $p = 0.25$) the new healed material is almost fully micro-cracked by the time the strain reaches the original unloading strain. In contrast to the other parameters, changing the

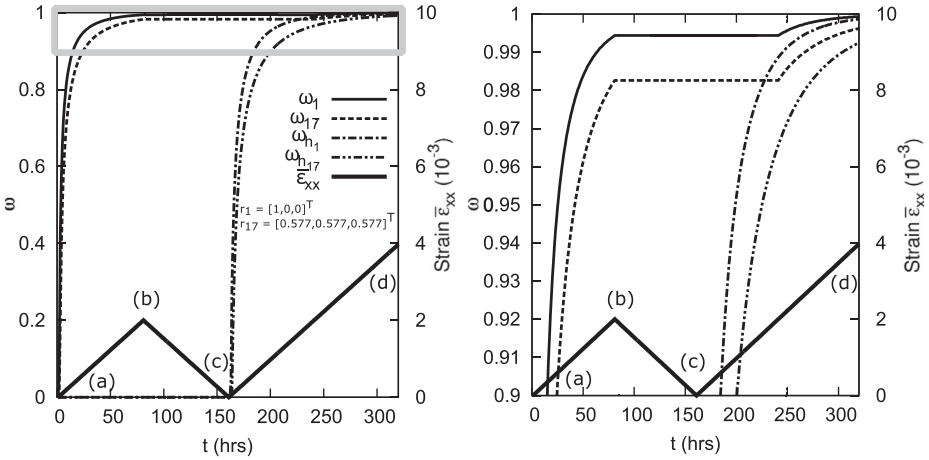

Fig. 6. Micro-cracking parameter response.

Table 3
Composition of concrete.

Material	Example 1 S1BC (kg/m^3)	Example 2 SSC (kg/m^3)	Example 3 UHPC (kg/m^3)
Cement (CEM1 52.5N)	-	366.2	1003.6
Cement (CEM1 II/B-V 32.5R)	396.7	-	-
Coarse aggregate	1110.7	1051.3	-
Sand	714.0	722.7	1104.0
Water	178.5	174.1	160.6
Micro-silica fume	-	36.6	188.2
Crushed quartz	-	-	62.7
Superplasticiser	-	2.0	5.0
w/c ratio	0.45	0.475	0.16

relative stiffness (B) of the healed material has a comparatively minor impact on the model response, as shown in Fig. 7d.

The relative simplicity of this micromechanical healing model combined with the fact that it requires a small number of physically meaningful parameters suggest that it is suitable for simulating a wide range of two-phase cementitious materials. Indeed, the model is capable of representing multi-directional 3D prescribed stress or strain increments. An example is given in Fig. 8 where a material is strained under confined conditions. Fig. 8a shows how a cementitious material is first compressed in the y-y and z-z directions to a predetermined stress ($\bar{\sigma}_{yy} = \bar{\sigma}_{zz} = -1N/mm^2$) and then prescribed a cyclic uniaxial strain in the x-x direction ($\bar{\varepsilon}_{xx}$). The healing is also assumed to take place at point c on the graphs in Fig. 8. Fig. 8c shows how the increase in confinement reduces the effects of healing on the peak post-healing stress compared to the reference model.

5. Comparison with experimental data

5.1. Introduction

Examples are now used to illustrate the performance of the healing model as implemented in a layered beam program (See Appendix B). The examples use data from two experimental programmes of work on self-healing in concrete. The first example considers experiments undertaken by the authors in Cardiff (Davies, 2014), in which the healing behaviour of cracks in notched concrete beams specimens were evaluated (S1BC). Examples 2 and 3 employ data from the test series undertaken by Granger et al. (2007b), in which standard strength concrete (SSC) and ultra high performance cement (UHPC) beams were loaded and then healed. All beams were tested under three point flexural bending and results given in terms of load against crack mouth opening displacement (CMOD). The typical experimental set-up for each example is illustrated in Fig. 9. The concrete composition of all examples are given in Table 3 and the experimental set-up dimensions, material properties along with key model parameters used are shown in Table 4. There was a significant discrepancy between the experimental and numerical initial 'elastic' responses for the UHPC specimens. This suggests that the notching procedure led to some micro-cracking, which caused a reduction in the initial stiffness. We therefore back-calculated an initial degree of micro-cracking such that the initial responses approximately agreed.

5.2. Examples

5.2.1. Example 1 autogenous healing S1BC

The experimental procedure, which includes details of the programme, specimen preparation, testing and results are presented in the PhD thesis by Davies (2014). The work included examining natural cracks, preformed narrow notches in concrete beams and the development of healing with time in preformed narrow notched mortar beams. Set 1 Beam C (S1BC) represents a typical 28 days autogenous healing response and is used for comparison with the micromechanical model. This beam was first tested 24 hours after casting, a natural crack was formed and the CMOD reached 0.3mm. After unloading, the beam was stored under water for 28 days to allow healing to occur before re-testing and re-loading.

The micromechanical model simulates the test by using measured material strength parameters. Fig. 10 presents the experimental pre-healing (initial loading) (Exp. Pre-H) and post-healing (second loading) (Exp. Post-H) results compared with the micromechanical model pre-healing (Mod. Pre-H) and post-healing (Mod. Post-H) results. The figure shows that the numerical model satisfactorily represents the experimental behaviour. It is noted that by using measured strength and stiffness parameters appropriate to the time of loading, the effects of strength and stiffness increases in uncracked ligaments of the specimens on post-healed responses were naturally taken into account. The specific issue of the effect on apparent healing indices of on-going curing in uncracked ligaments of fracture-healing tests is the subject of a separate paper by the authors (Davies and Jefferson, 2017).

5.2.2. Example 2 autogenous healing SSC

The second example is chosen from the standard strength concrete (SSC) beam results presented by Granger (2006) (also described in Granger et al. (2007a)). Experiments were carried out with water and air curing regimes with the time of healing ranging between 1 and 20 weeks. The specific example chosen

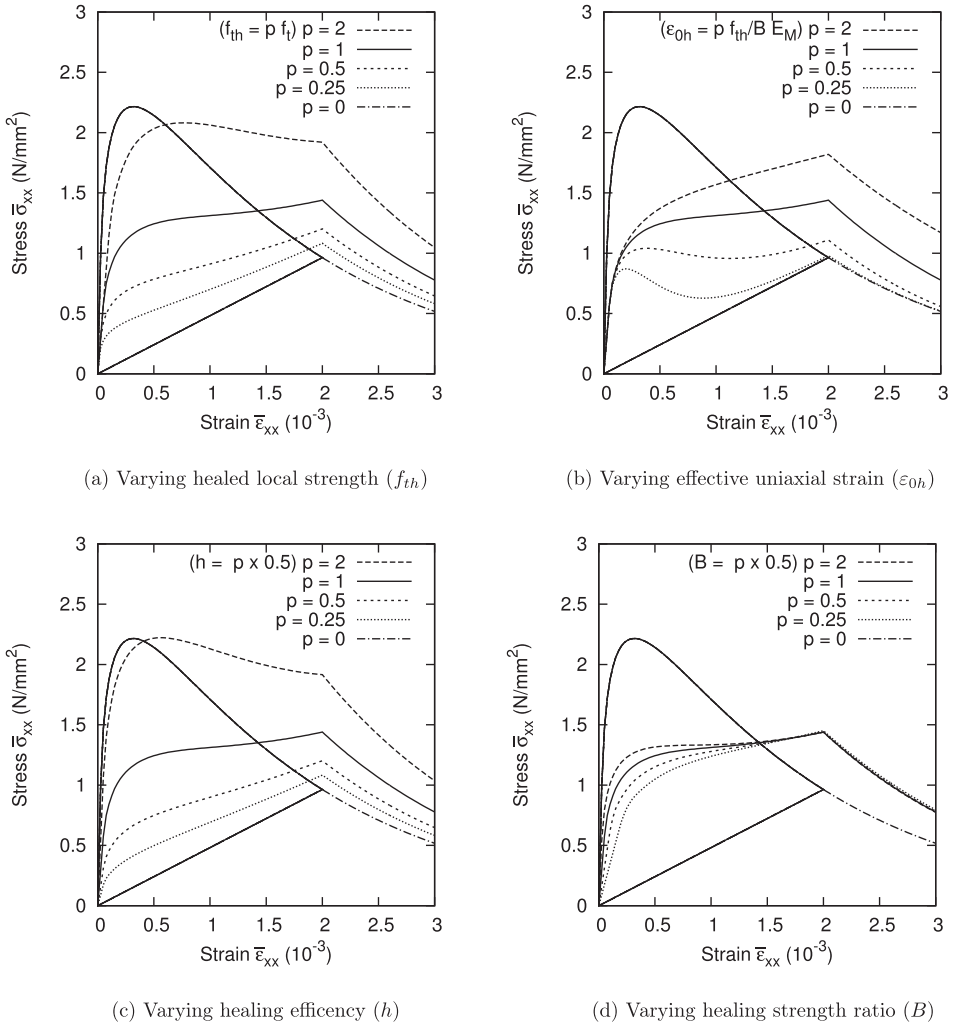

(a) Varying healed local strength (f_{th})

(b) Varying effective uniaxial strain (ε_{0h})

(c) Varying healing efficency (h)

(d) Varying healing strength ratio (B)

Fig. 7. Parametric study of model performance.

Table 4
Experimental set-up dimensions, material properties and key model parameters.

Example	L (mm)	h_b (mm)	b_b (mm)	Beam length L_1 (mm)	$nlay$	h_n (mm)	w_c (mm)
1. S1BC	200	75	75	255	100	5	5
2. SSC	400	100	50	500	100	20	5
3. UHPC	400	100	50	500	100	20	5
	f_M	E_M (N/mm^2)	ν_M	f_Ω	E_Ω (N/mm^2)	ν_Ω	f_t (N/mm^2)
1. S1BC	0.463	20,000	0.15	0.537	55,000	0.25	0.475
2. SSC	0.553	22,500	0.15	0.447	45,000	0.25	8.0
3. UHPC	0.583	24,000	0.15	0.417	57,000	0.25	10.0
	ε_t	ε_0	f_{th} (N/mm^2)	ε_{th}	ε_{0h}	B	h
1. S1BC	1.22 $x10^{-5}$	0.035	0.475	2.45 $x10^{-5}$	0.035	0.5	0.8
2. SSC	1.07 $x10^{-3}$	0.020	2.4	4.27 $x10^{-4}$	0.010	0.75	0.4
3. UHPC	1.25 $x10^{-3}$	0.031	8.0	1.18 $x10^{-3}$	0.031	0.85	0.2

is beam number 4 sample 1. This beam was cured for two days and then subjected to thermal treatment to accelerate ageing and pozzolanic reactions before the first loading. The specimens were loaded beyond the peak stress level and subsequently unloaded until the CMOD reached 0.05 mm. This beam was cured in water for 20 weeks before reloading.

Fig. 11 shows the experimental and numerical model results for example 2. The post-healing experimental loading curve (Exp. Post-H) displays two straight gradient sections which are reflected in the micromechanical model response (Mod. Post-H).

5.2.3. Example 3 autogenous healing UHPC

Granger (2006) also carried out self-healing experiments using ultra high performance concrete (UHPC) formed from reactive powder concrete. The mix proportions for the UHPC were not given in the paper; however, a typical UHPC composition was chosen for the numerical model (Mounanga et al., 2012) assuming that there was no coarse aggregate present in the mix. The example chosen is presented in Figure 2.13 and 3.5 (Granger, 2006). These beams received the same thermal treatment as SSC, were

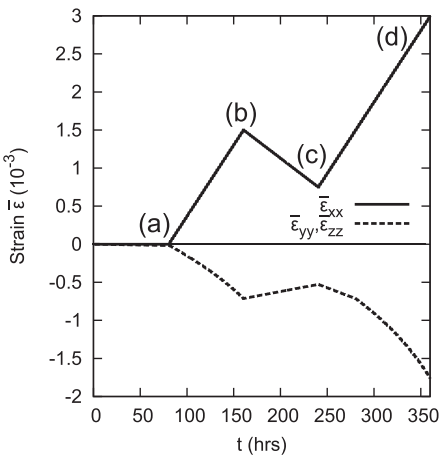

(a) Uniaxial tensile strain

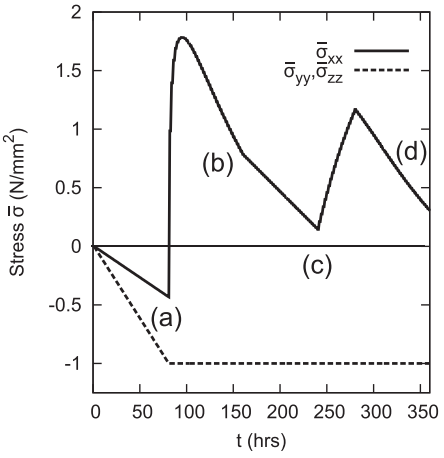

(b) Stress response

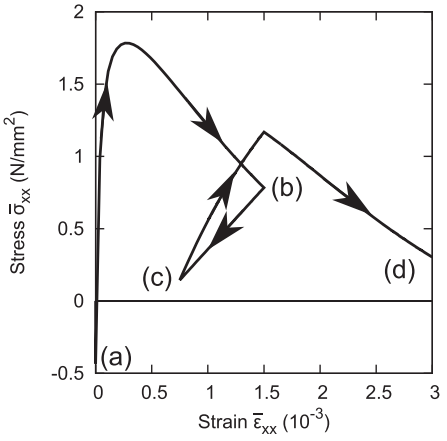

(c) Strain stress response

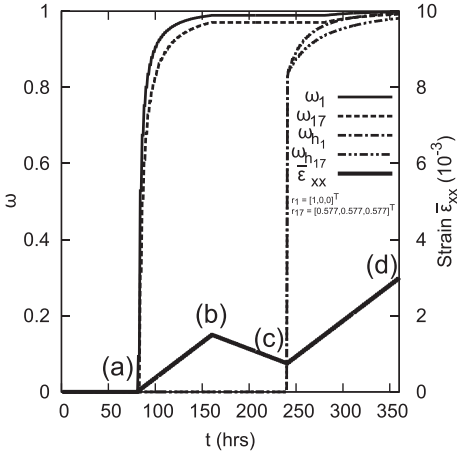

(d) Micro-cracking parameter response

Fig. 8. Model response with confined stress in the y–y and z–z direction.

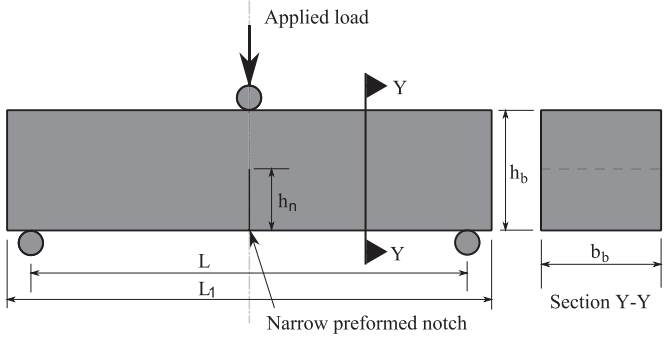

Fig. 9. Specimen general arrangement.

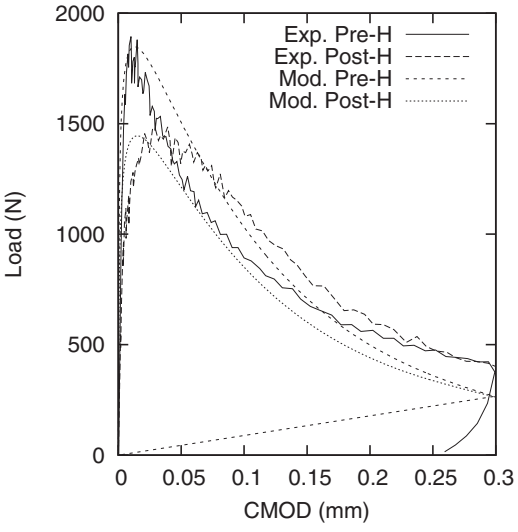

Fig. 10. Load CMOD plots for experimental data (Exp.) and micromechanical model (Mod.) S1BC.

loaded leaving a residual 10 μ*m* CMOD and then cured in water and air respectively for 20 weeks.

Fig. 12 shows the load CMOD comparisons between experimental and numerical model results for the pre-healed stage and for the post-healing stages for both the water and air cured beams. The curing in air results are presented (Exp. Air-H and Mod. Air-H) and show that no healing took place since the maximum load upon re-loading does not exceed the pre-healed load at the maximum displacement.

These comparisons with experimental data suggest that the model can be used for a range of cementitious materials with minimal parameter fitting. For the present examples, it was considered

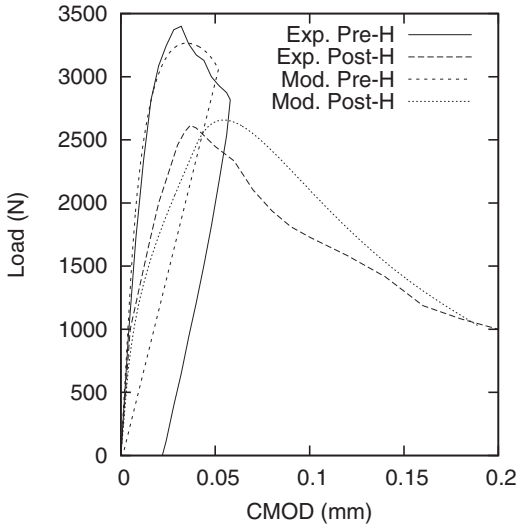

Fig. 11. Load CMOD plots for experimental data (Exp.) and micromechanical model (Mod.) SSC .

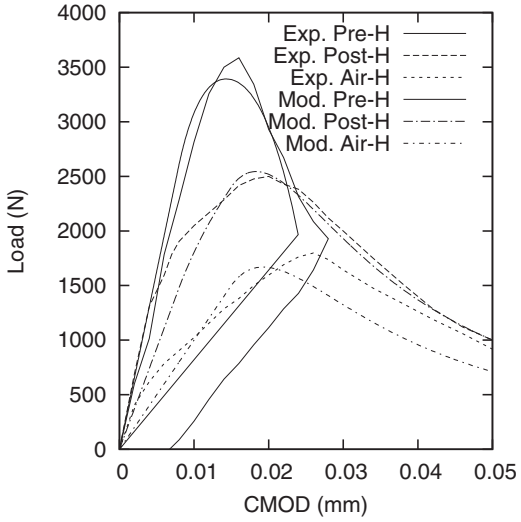

Fig. 12. Load CMOD plots for experimental data (Exp.) and micromechanical model (Mod.) UHPC.

reasonable to assume that all of the healing occurred in a single time step. However, there are other cases for which it would be more accurate to spread the healing process over a number of time steps. The current model does not allow for this, in its present form, but could readily be adapted to include gradual healing processes.

6. Conclusions

- A two phase composite micro-mechanical constitutive model, that includes anisotropic micro-cracking, provides a natural basis for the development of a model for cementitious materials that includes self-healing behaviour.
- The application of the solidification principle to micro-crack healing provides an effective means of simulating self-healing behaviour within a micro-mechanical model.
- The new micro-mechanical model described in this paper is able to simulate the characteristic damage-healing behaviour observed in experiments on samples formed from cementitious composite materials, including;
  - the partial or complete recovery of strength and stiffness of a micro-cracked region,
  - the formation of (healing) material in a stress free state, such that the stress state does not change at the instant of healing,
  - the development of permanent strains resulting from micro-cracking filling,
  - continued damage (or micro-cracking) of a healed region.

Acknowledgement

The writers gratefully acknowledge the financial support for this study given by the Engineering and Physical Sciences Research Council (EPSRC) (Project Ref. EP/K026631/1).

All data created during this research are openly available from the Cardiff University data archive at http://dx.doi.org/10.17035/d.2015.0008104212.

Appendix A. Unit direction vectors and weightings for sampling directions

Table A.1
Directional micro-cracking parameters.

Sampling direction	Unit direction vector	Weighting (w_i)
r_1	(1, 0, 0)	0.0254
r_2	(0, 1, 0)	0.0127
r_3	(0, 0, 1)	0.0127
r_4	(0, −1, 0)	0.0127
r_5	(0, 0, −1)	0.0127
r_6	(0.707, −0.707, 0)	0.04515
r_7	(0.707, 0.707, 0)	0.04515
r_8	(0, −0.707, −0.707)	0.02257
r_9	(0, −0.707, 0.707)	0.02257
r_{10}	(0, 0.707, −0.707)	0.02257
r_{11}	(0, 0.707, 0.707)	0.02257
r_{12}	(0.707, 0, −0.707)	0.04515
r_{13}	(0.707, 0, 0.707)	0.04515
r_{14}	(0.577, −0.577, −0.577)	0.04219
r_{15}	(0.577, −0.577, 0.577)	0.04219
r_{16}	(0.577, 0.577, −0.577)	0.04219
r_{17}	(0.577, 0.577, 0.577)	0.04219
r_{18}	(0.302, −0.302, −0.905)	0.04035
r_{19}	(0.302, 0.302, −0.905)	0.04035
r_{20}	(0.302, −0.905, −0.302)	0.04035
r_{21}	(0.302, −0.905, 0.302)	0.04035
r_{22}	(0.302, −0.302, 0.905)	0.04035
r_{23}	(0.302, 0.302, 0.905)	0.04035
r_{24}	(0.905, −0.302, −0.302)	0.04035
r_{25}	(0.905, −0.302, 0.302)	0.04035
r_{26}	(0.905, 0.302, −0.302)	0.04035
r_{27}	(0.905, 0.302, 0.302)	0.04035
r_{28}	(0.302, 0.905, −0.302)	0.04035
r_{29}	(0.302, 0.905, 0.302)	0.04035

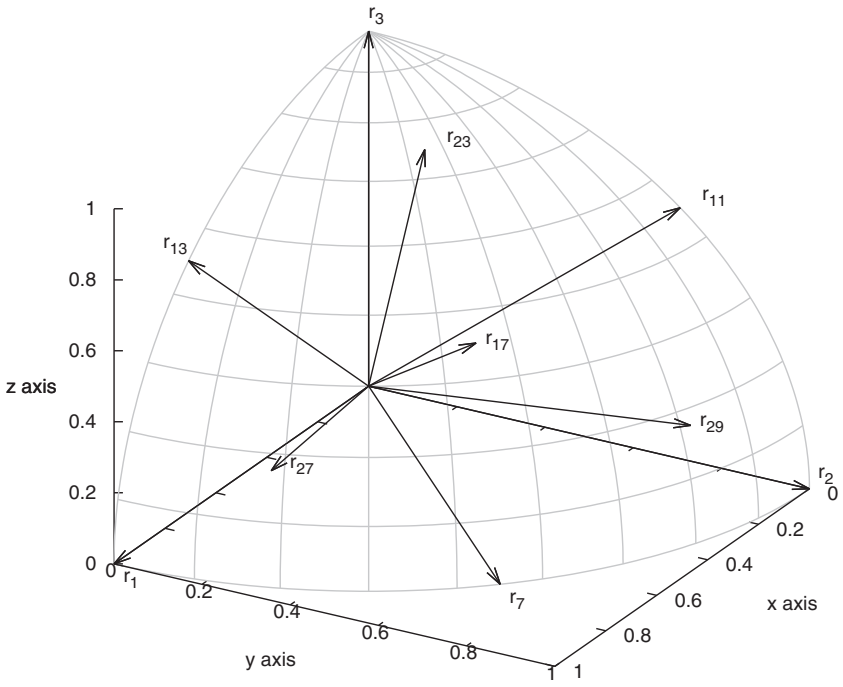

Fig. A.1. Selected illustration of sampling directions.

Appendix B. Layered beam model

The layered beam model (Owen and Hinton, 1980) computes the stiffness of Timoshenko beam elements using a layered approach. The coupled relationship between the generalised forces (axial load and moment) and deformations (mean strain and curvature) is given by;

$$\begin{Bmatrix} N \\ M \end{Bmatrix} = \begin{bmatrix} \sum_{j=1}^{nlay} E_{s_j} \cdot b_{b_j} \cdot \Delta z_j & \sum_{j=1}^{nlay} E_{s_j} \cdot b_{b_j} \cdot z_j \cdot \Delta z_j \\ \sum_{j=1}^{nlay} E_{s_j} \cdot b_{b_j} \cdot z_j \cdot \Delta z_j & \sum_{j=1}^{nlay} E_{s_j} \cdot b_{b_j} \cdot z_j^2 \Delta z_j \end{bmatrix} \cdot \begin{Bmatrix} \bar{\varepsilon} \\ \phi \end{Bmatrix} \tag{B.1}$$

in which j is the layer number, z is the vertical coordinate at the centre of a layer, Δz is the thickness of a layer. b_{b_j} is the width of the layer, $\bar{\varepsilon}$ is the average strain at the neutral axis, ϕ is the curvature, N is the axial load, M is the moment and E_{s_j} is the secant modulus of the layer.

The strain ($\boldsymbol{\varepsilon}$) in each layer (j) is given by;

$$\varepsilon_j = \bar{\boldsymbol{\varepsilon}} - \phi \cdot z_j \tag{B.2}$$

and the secant Young's Modulus (E_s) is obtained from the micromechanical model, see Eq. (16).

In the examples presented in this paper, the strain localises to a small central element chosen to be equal in length to the width of the fracture process zone w_c (i.e. 3 times the size of the coarse aggregate particles). Once localization has occurred the load (P) vs CMOD (crack mouth opening displacement) relationship may be obtained from;

$$P = \frac{M}{L} \tag{B.3}$$

$$CMOD = w_c(\bar{\varepsilon} + \phi \cdot h_b) \tag{B.4}$$

where h_b is the distance (taken as a positive number) from the neutral axis to the level at which the CMOD is measured. The curvature is obtained from the change of slope across the element ($\Delta\Theta$), given by;

$$\phi = \frac{\Delta\Theta}{w_c} \tag{B.5}$$

The combined micromechanical and layered beam model was implemented in a Mathcad (2010) sheet.

References

Abu Al-Rub, R.K., Darabi, M.K., 2012. A thermodynamic framework for constitutive modeling of time- and rate-dependent materials. part i: theory. Int. J. Plast. 34, 61–92. doi:10.1016/j.ijplas.2012.01.002.

Abu Al-Rub, R.K., Darabi, M.K., Little, D.N., Masad, E.A., 2010. A micro-damage healing model that improves prediction of fatigue life in asphalt mixes. Int. J. Eng. Sci. 48 (11), 966–990. doi:10.1016/j.ijengsci.2010.09.016.

Alfredsson, K.S., Stigh, U., 2004. Continuum damage mechanics revised: a principle for mechanical and thermal equivalence. Int. J. Solids Struct. 41 (15), 4025–4045. doi:10.1016/j.ijsolstr.2004.02.052.

Barbero, E.J., Greco, F., Lonetti, P., 2005. Continuum damage-healing mechanics with application to self-healing composites. Int. J. Damage Mech. 14, 51–81. doi:10.1177/1056789505045928.

Baroghel-Bouny, V., Thiéry, M., Wang, X., 2011. Modelling of isothermal coupled moisture-ion transport in cementitious materials. Cem. Concr. Res. 41 (8), 828–841. doi:10.1016/j.cemconres.2011.04.001.

Bažant, Z.P., Prasannan, S., 1989. Solidification theory for concrete creep: i. formulation. J. Eng. Mech. 115 (8), 1691–1703.

Benveniste, Y., 1987. A new approach to the application of Mori–Tanaka's theory in composite materials. Mech. Mater. 6 (2), 147–157.

Budiansky, B., O'Connell, R., 1976. Elastic-moduli of a cracked solid. Int. J. Solids Struct. 12 (2), 81–97.

Darabi, M.K., Abu Al-Rub, R.K., Little, D.N., 2012. A continuum damage mechanics framework for modeling micro-damage healing. Int. J. Solids Struct. 49 (3–4), 492–513. doi:10.1016/j.ijsolstr.2011.10.017.

Darabi, M.K., Abu Al-Rub, R.K., Masad, E.A., Little, D.N., 2013. Constitutive modeling of fatigue damage response of asphalt concrete materials with consideration of micro-damage healing. Int. J. Solids Struct. 50 (19), 2901–2913. doi:10.1016/j.ijsolstr.2013.05.007.

Davies, R., Jefferson, A., 2014. The simulation of inelastic matrix strains in cementitious materials using micromechanical solutions. Eng. Fract. Mech. doi:10.1016/j.engfracmech.2014.10.010.

Davies, R., Jefferson, A., 2017. The simulation of inelastic matrix strains in cementitious materials using micromechanical solutions. Cem. Concr. Compos.. under review

Davies, R.E., 2014. Micromechanical modelling of self-healing cementitious materials. Cardiff University Thesis.

Eshelby, J.D., 1957. The determination of the elastic field of an ellipsoidal inclusion, and related problems. Proc R Soc Lond A Math Phys Sci 241 (1226), 376–396.

Gardner, D., Jefferson, A., Hoffman, A., Lark, R., 2014. Simulation of the capillary flow of an autonomic healing agent in discrete cracks in cementitious materials. Cem. Concr. Res. 58, 35–44. doi:10.1016/j.cemconres.2014.01.005.

Gawin, D., Pesavento, F., Schrefler, B.A., 2008. Modeling of cementitious materials exposed to isothermal calcium leaching, considering process kinetics and advective water flow. part 1: theoretical model. Int. J. Solids Struct. 45 (25–26), 6221–6240. doi:10.1016/j.ijsolstr.2008.07.010.

Granger, S., 2006. Caracterisation experimentale et modelisation du phenomene d'auto-cicatrisation des fissures dans les betons. L'École Centrale de Nantes et l'Université de Nantes PhD.

Granger, S., Loukili, A., Pijaudier-Cabot, G., Chanvillard, G., 2005. Mechanical characterization of the self-healing effect of cracks in ultra high performance concrete (UHPC). In: Proceedings Third International Conference on Construction Materials, Performance, Innovations and Structural Implications, ConMat, 5, pp. 22–24.

Granger, S., Loukili, A., Pijaudier-Cabot, G., Chanvillard, G., 2007. Experimental characterization of the self-healing of cracks in an ultra high performance cementitious material: mechanical tests and acoustic emission analysis. Cem. Concr. Res. 37 (4), 519–527.

Granger, S., Pijaudier-Cabot, G., Loukili, A., 2007. Mechanical behavior of self-healed ultra high performance concrete: from experimental evidence to modeling. in Proc. FRAMCOS 6.

Hilloulin, B., Grondin, F., Matallah, M., Loukili, A., 2014. Modelling of autogenous healing in ultra high performance concrete. Cem. Concr. Res. 61–62, 64–70. doi:10.1016/j.cemconres.2014.04.003.

Huang, H., Ye, G., 2012. Simulation of self-healing by further hydration in cementitious materials. Cem. Concr. Compos. 34 (4), 460–467.

Jefferson, A.D., 2003. Craft- a plastic-damage-contact model for concrete. i. model theory and thermodynamic considerations. Int. J. Solids Struct. 40, 5973–5999.

Jefferson, A.D., Bennett, T., 2007. Micro-mechanical damage and rough crack closure in cementitious composite materials. Int. J. Numer. Anal. Methods Geomech. 31 (2), 133–146.

Ju, J.W., Sun, L.Z., 1999. A novel formulation for the exterior-point eshelby's tensor of an ellipsoidal inclusion. J. Appl. Mech. 66 (2), 570–574. doi:10.1115/1.2791090.

Mathcad, 2010. Mathcad help manual. http://www.ptc.com/product/mathcad [Accessed: 18 October 2013]. Version 15.0.

Mergheim, J., Steinmann, P., 2013. Phenomenological modelling of self-healing polymers based on integrated healing agents. Comput. Mech. 52 (3), 681–692. doi:10.1007/s00466-013-0840-0.

Miao, S., Wang, M., Schreyer, H., 1995. Constitutive models for healing of materials with application to compaction of crushed rock salt. J. Eng. Mech. 121 (10), 1122–1129. doi:10.1061/(ASCE)0733-9399(1995)121:10(1122).

Mihai, I.C., Jefferson, A.D., 2011. A material model for cementitious composite materials with an exterior point eshelby microcrack initiation criterion. Int. J. Solids Struct. 48, 3312–3325. doi:10.1016/j.ijsolstr.2011.08.001.

Mihai, I.C., Jefferson, A.D., 2013. Smoothed contact in a micromechanical model for cement bound materials. Comput. Struct. 118, 115–125. doi:10.1016/j.compstruc.2012.11.002.

Mori, T., Tanaka, K., 1973. Average stress in matrix and average elastic energy of materials with misfitting inclusions. Acta. Metall. 21 (5), 571–574.

Mounanga, P., Cherkaoui, K., Khelidj, A., Courtial, M., Noirfontaine, M.-N.d., Dunstetter, F., 2012. Extrudable reactive powder concretes: hydration, shrinkage and transfer properties. Eur. J. Environ. Civil Eng. 16 (sup1), s99–s114. doi:10.1080/19648189.2012.681961.

Nemat-Nasser, S., Hori, M., 1999. Micromechanics: overall properties of heterogeneous materials. Elsevier, Amsterdam; New York.

Owen, D.R.J., Hinton, E., 1980. Finite elements in plasticity: theory and practice. Pineridge Press Ltd, Swansea.

Perelmuter, M., 2013. Bridged crack approach to model materials self-healing.

Pichler, B., Hellmich, C., A. Mang, H., 2007. A combined fracture micromechanics model for tensile strain softening in brittle materials, based on propagation of interacting microcracks. Int. J. Numer. Anal. Methods Geomech. 31 (2), 111–132.

Reinhardt, H.W., 1984. Fracture mechanics of an elastic softening material like concrete. HERON 29 (2), 5–34.

Remmers, J.J., de Borst, R., 2008. Numerical Modelling of Self Healing Mechanisms. In: Self Healing Materials. Springer, pp. 365–380.

de Rooij, M.R., Van Tittelboom, K., De Belie, N., Schlangen, E., 2013. Self-healing phenomena in cement-Based materials: state-of-the-art report of RILEM technical committee 221-SHC: self-Healing phenomena in cement-Based materials. Springer, Bagneux, France.

Schimmel, E. C., Remmers, J. J. C., 2006. Development of a Constitutive Model for Self-Healing Materials. Delft Aerospace Computational Science, Report DACS-06-003.

Schlangen, E., Ter Heide, N., Van Breugel, K., 2006. Crack healing of early age cracks in concrete. ECF16. Alexandroupolis, Greece.

Stroud, A., 1972. Approximate Calculation of Multiple Integrals. Prentice Hall, Englewood Cliffs, N.J.

Van Tittelboom, K., De Belie, N., 2013. Self-healing in cementitious materials—a review. Materials (Basel) 6 (6), 2182–2217.

Voyiadjis, G.Z., Shojaei, A., Li, G., 2011. A thermodynamic consistent damage and healing model for self healing materials. Int. J. Plast. 27 (7), 1025–1044. doi:10.1016/j.ijplas.2010.11.002.

Voyiadjis, G.Z., Shojaei, A., Li, G., Kattan, P., 2012. Continuum damage-healing mechanics with introduction to new healing variables. Int. J. Damage Mech. 21 (3), 391–414. doi:10.1177/1056789510397069.

Ye, G., van Breugel, K., 2007. Potential use of HYMOSTRUC cement hydration model for self-healing of microcracks in cementitious materials. In: Proceedings of the First International Conference on Self Healing Materials. Noordwijk aan Zee, The Netherlands.